Effect of Magnetic Island Associated with Neoclassical Tearing Modes on Plasma Rotation in JT-60U

Akihiko ISAYAMA, Go MATSUNAGA, Yasutomo ISHII, Yoshiteru SAKAMOTO, Shinichi MORIYAMA, Yutaka KAMADA, Takahisa OZEKI and the JT-60 team

Japan Atomic Energy Agency, Naka, Ibaraki 311-0193, Japan

(Received 9 July 2010 / Accepted 25 August 2010)

This paper describes the dependence of the rotation frequency of an $m/n = 2/1$ neoclassical tearing mode (NTM) on its magnetic island width in JT-60U (m and n are the poloidal and toroidal mode numbers, respectively). Throughout the experiments, the island width is actively controlled by changing the location of the electron cyclotron current drive (ECCD), based on the fact that aligned ECCD and misaligned ECCD make the NTM islands shrink and grow, respectively. The NTM frequency was found to gradually decrease with the increasing island width. While the frequency is 5.5 kHz for zero island width, it is 3 kHz for the full island width of about 15% of the plasma minor radius. Also, the mode frequency suddenly decreases (typically by 80%) shortly after the misaligned ECCD, during which the increment in the island width is only less than 10%. A sudden increase in the mode frequency is observed shortly after the ECCD turnoff, which is nearly the reverse process of the sudden decrease, but with a hysteresis in the island width at which downward and upward frequency changes occur. The downward frequency change occurs when the frequency decreases to about half of that without the NTM.

© *2010 The Japan Society of Plasma Science and Nuclear Fusion Research*

Keywords: neoclassical tearing mode, magnetic island, electron cyclotron current drive, tokamak, JT-60U

DOI: 10.1585/pfr.5.037

1. Introduction

A neoclassical tearing mode (NTM) refers to a magnetohydrodynamic instability that appears in a high-β plasma with positive magnetic shear; it is characterized by the formation of magnetic islands. Here, β is the ratio of the plasma pressure to the magnetic pressure. Since NTMs degrade the plasma performance, it is necessary to control them in order to sustain a high-β plasma. Of the possible mode numbers, an NTM with $m/n = 2/1$ must be suppressed since it causes mode locking and can lead to disruption. Here, m and n are the poloidal and toroidal mode numbers, respectively. Control of NTMs by current drive using electron cyclotron (EC) waves, the so-called electron cyclotron current drive (ECCD), is considered the most promising method because current drives can be highly localized and an accurate control of the ECCD location is feasible.

Suppression of NTMs with $m/n = 3/2$ and $2/1$ by using ECCD has been demonstrated in JT-60U: real-time identification of the mode location, optimization of the ECCD location, and complete stabilization of an NTM [1]; avoidance of NTM onset by preemptive ECCD, where EC waves are injected to the anticipated mode location [2]; and NTM stabilization by power-modulated EC waves in synchronization with the NTM rotation [3]. Similar experiments were also performed in ASDEX-U [4] and DIII-D [5], and a control scheme for real-time NTM stabilization has also made considerable progress.

The frequency of 'classical' tearing mode islands decreases and locks as the strength of external magnetic perturbations is increased. The threshold for such mode locking, which typically appears at a low density, has been investigated in detail [6–8]. In JT-60U experiments on NTMs, a similar mode locking, in which the mode frequency becomes very low or zero owing to magnetic island formation, has been observed for NTM islands even without external magnetic perturbations. In this case, the mode locking is considered to be caused by the interaction between the magnetic islands and the conductive structure surrounding the plasma. However, detailed investigation on the island behavior near the mode locking threshold has not been conducted before. Thus, it is important to clarify the effect of NTM islands on the plasma rotation and to avoid mode locking, because the threshold island width for mode locking is expected to be very low in ITER [9].

JT-60U has the capability of investigating this issue by detailed scanning of the ECCD location. It was previously demonstrated that NTM islands expand (i.e., are destabilized) when the ECCD location is misaligned from the mode rational surface by about the full island width, and that the islands shrink when the ECCD misalignment is less than about half the island width [10]. Compared with the locked mode experiments using external coils, the experiments using ECCD are unique in the sense that NTM islands are directly stabilized or destabilized by the ECCD,

author's e-mail: isayama.akihiko@jaea.go.jp

© 2010 The Japan Society of Plasma Science and Nuclear Fusion Research

and thus, the conditions at other plasma locations are not directly affected.

This paper describes the effect of $m/n = 2/1$ NTM islands on the toroidal rotation velocity in JT-60U. Section 2 describes the change in the toroidal rotation velocity during NTM stabilization and destabilization by ECCD. Observations of rapid changes in the mode frequency are described in Sec. 3. Finally, a summary and discussion are presented in Sec. 4.

2. Change in NTM Frequency during ECCD

Typical discharge and plasma cross sections of NTM stabilization/destabilization experiments are shown in Fig. 1. The plasma parameters are as follows: plasma current I_p =1.5 MA, toroidal field B_t = 3.7 T, major radius R = 3.18 m, safety factor at 95% flux surface q_{95} = 3.9, and line-averaged electron density $\bar{n}_e \sim 3 \times 10^{19}\,\mathrm{m}^{-3}$. In this series of discharges, neutral beams (NBs) of about 20 MW are injected simultaneously to raise the beta value rapidly and destabilize an $m/n = 2/1$ NTM. At $t = 5.7$ s, an $m/n = 2/1$ NTM appears and the beta value decreases. At $t = 7.0$ s, the power of the NBs is decreased to 11.6 MW, and their injection pattern is changed from balanced injection to counter-injection so that the NTM can be measured at several kHz. The mode frequency is low for about 1 s after the power-down, and it starts to increase at $t \sim 8$ s. The mode frequency saturates at about 5 kHz. At $t = 9.5$ s, electron cyclotron waves, with a frequency and power of 110 GHz and 1.9 MW, respectively, are injected from the low-field side (see Fig. 1 (d) for the injection geometry). In this discharge, in which misaligned EC waves are injected, the 2/1 mode is completely stabilized at $t \sim 12.6$ s, i.e., 3 s after the ECCD. The mode frequency increases very slightly after the EC wave injection. According to the EC-Hamamatsu code [11], the ECCD profile has a peak at about 0.6 with a full-width at half-maximum of about 0.08 in units of volume-averaged minor radius, ρ. Also, the ACCOME [12] and EC-Hamamatsu codes show that the peak EC-driven current density is comparable to the bootstrap current density at the deposition location, and its value is about 3.5 MA/m^2.

Figure 2 (a) shows the temporal evolution of the toroidal rotation velocity, V_t, measured by charge exchange recombination spectroscopy (CXRS) from $t = 7.0$ s, at which the NB power was stepped down, to 8.3 s, at which the frequency of the 2/1 mode saturated. The 2/1 mode is located at $\rho \sim 0.6$. At $t = 7.0$ s, V_t at $\rho \gtrsim 0.5$ remains low while V_t at $\rho \lesssim 0.5$ is negatively larger in more central regions. As time increases, V_t at $\rho \sim 0.2$ continuously increases in the counter-direction and saturates at $t = 8$ s. On the other hand, V_t at $\rho \sim 0.6$ starts to increase at $t \sim 8$ s, similar to the evolution of the 2/1 mode frequency shown in Fig. 1 (c). The relationship between the frequency of the 2/1 mode and V_t at $\rho \sim 0.6$ is shown in Fig. 2 (b), where

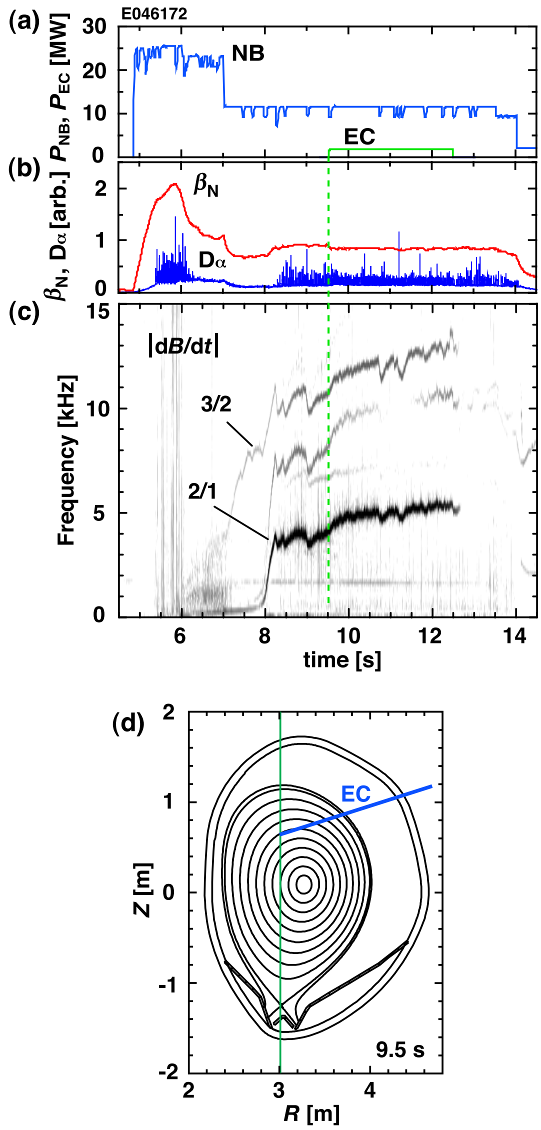

Fig. 1 (a) Injection power of NBs and EC waves, (b) normalized beta and D_α emission intensity, (c) frequency spectrum of magnetic perturbations and (d) plasma cross section and ray trajectory of EC waves. Cold resonance surface for the 110 GHz EC waves is located at R = 3.0 m.

the rotation frequency evaluated from the rotation velocity, $-V_t(\rho \sim 0.6)/(2\pi R_{CXRS})$, is also shown for comparison (R_{CXRS} is the measurement point of the CXRS diagnostic, and the minus sign indicates counter-rotation). As shown in this figure, V_t is well fitted to an offset linear function with a gradient of about $n/(2\pi R_{CXRS})$. Although a similar degree of offset is seen with both co- and counter-rotation, the reason for the offset has not been clarified yet. Possible candidates are (a) the existence of poloidal rotation, (b) deviation of the mode rotation velocity from the plasma rotation velocity, and (c) a discrepancy between the carbon rotation velocity measured by the CXRS diagnostic and the deuterium rotation velocity. Based on this information, the earlier increase in the 3/2 mode in shot E46172 (Fig. 1) can be explained by the earlier increase in the rotation velocity.

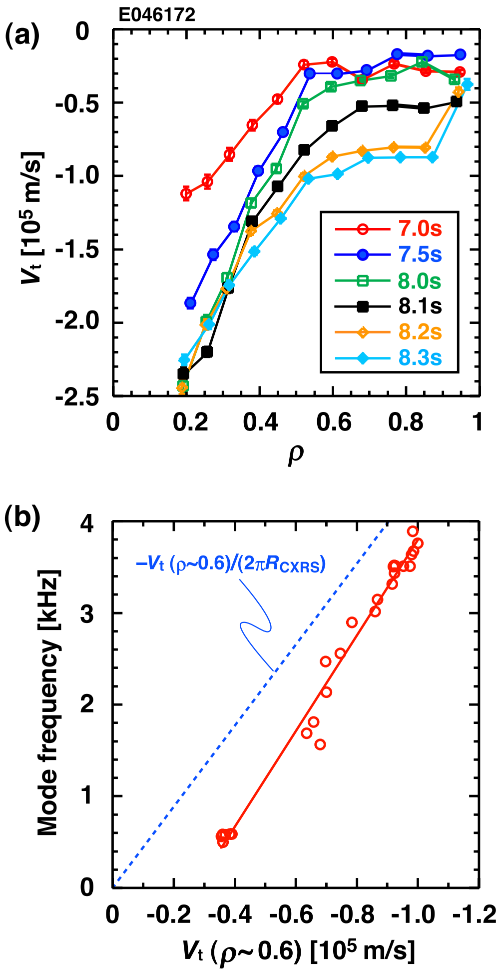

Fig. 2 (a) Evolution of toroidal rotation velocity profile and (b) frequency of the 2/1 mode as a function of toroidal rotation velocity at $\rho \sim 0.6$.

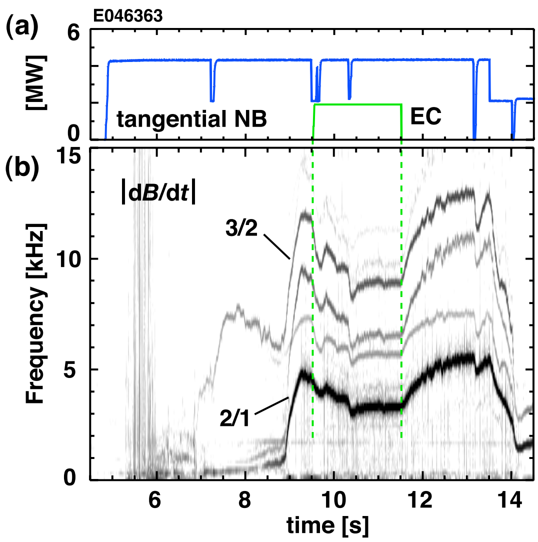

Fig. 3 (a) Injection power of NBs and EC waves and (b) frequency spectrum of magnetic perturbations. Discharge conditions are almost the same as those in E46172 (Fig. 1) except for the EC wave injection angle.

The temporal evolution of the frequency spectrum in a similar discharge is shown in Fig. 3. The discharge conditions are almost the same as those in shot E46172 except for the injection angle of the EC waves. The deposition location of the EC wave is misaligned by about the full island width, i.e., ~ 0.1 in units of normalized minor radius. Unlike shot E46172, the mode frequency of the 2/1 mode decreases after the EC wave injection and stays at about 3.2 kHz until the EC wave injection is turned off. After the turnoff, the mode frequency increases to that before the EC wave injection.

Figure 4 (a) compares the temporal evolution of the magnetic perturbation of the 2/1 mode in three discharges. As described above, the 2/1 mode is completely stabilized at t = 12.6 s in shot E46172. In shot E46367, where the ECCD alignment is better, the 2/1 mode is completely stabilized in about 2 s. In shot E46363, the mode amplitude increases with the ECCD and decreases after the EC wave injection turnoff at t = 11.5 s. Figure 4 (b) shows

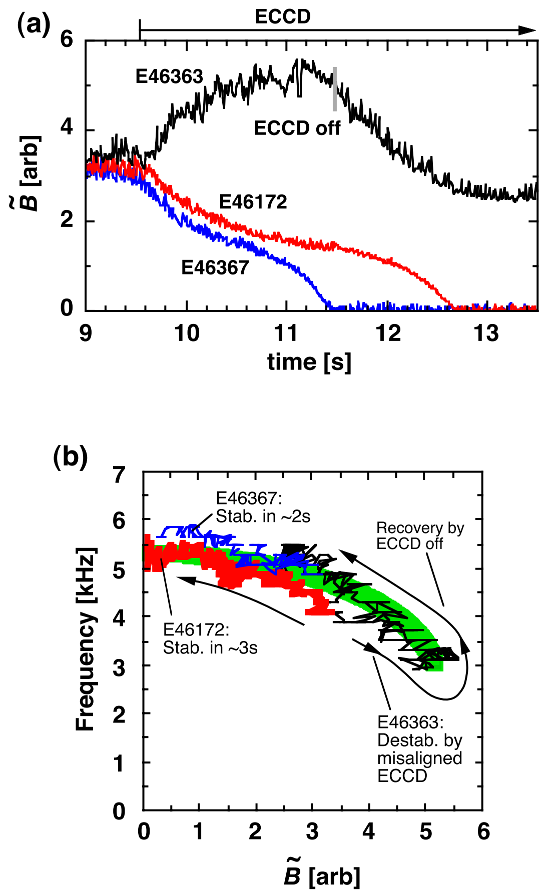

Fig. 4 (a) Temporal evolution of magnetic perturbation amplitude. (b) Evolution of NTM islands during the ECCD in mode amplitude-mode frequency space. In shot E46361, EC waves were turned off at t = 11.5 s. ECCD locations for E46367, E46172 and E46363 are calculated as ρ = 0.61, 0.64 and 0.46, respectively, and the island center is located at ρ = 0.59. Light bold line is a fitting function for the mode frequency.

the evolution of the NTM islands of these discharges in mode amplitude-mode frequency space. For NTM stabilization (shots E46172 and E46367), the mode frequency increases as the mode amplitude decreases with the ECCD. While the time to complete the stabilization differs in these discharges, the evolution is very similar. For NTM destabilization (shot E46363), the mode frequency decreases to about 3 kHz as the mode amplitude increases, and it increases after the EC wave injection turnoff by tracing a similar trajectory in a reverse order. These results show that the mode frequency has a weak negative dependence on the island width.

As shown in Fig. 3, a change in the mode frequency is also observed in the 3/2 NTM, which is located at $\rho \sim 0.5$. Figure 5 (a) shows the ratio of the mode frequency of the 2/1 mode, $f_{2/1}$, to that of the 3/2 mode, $f_{3/2}$, in shot E46363. If the plasma rotation slows down like that of a rigid body, this ratio will remain unchanged. At $t = 7.5$–8 s, the ratio is low because $f_{2/1}$ remains low, while $f_{3/2}$ has already started to increase. When the $f_{2/1}$ mode starts increasing, the ratio also increases and reaches about 0.4. Although the ratio would be 0.5 if the plasma were a rigid body, the ratio is lower than this because of the higher rotation velocity in the inner region of the plasma. During the ECCD, the ratio decreases to about 0.35, i.e., about 10% lower. After the EC wave injection is turned off,

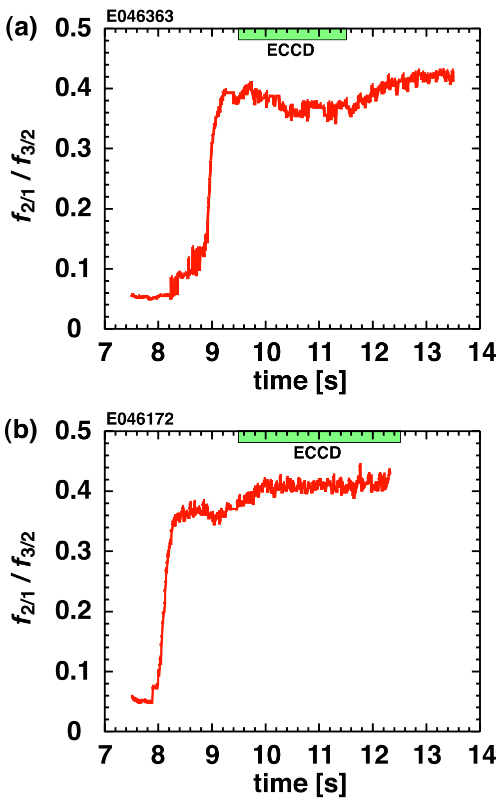

Fig. 5 Temporal evolution of the ratio of the 2/1 mode frequency to the 3/2 mode frequency in shots (a) E46363 and (b) E46172.

the ratio starts to increase to a value similar to that before the ECCD. The result shows that the deceleration by the ECCD has a stronger effect on the 2/1 rational surface. A similar plot of $f_{2/1}/f_{3/2}$ for shot E46172, where the 2/1 mode was completely stabilized, is shown in Fig. 5 (b). The value of $f_{2/1}/f_{3/2}$ does not decrease with the ECCD; rather, it seems to increase very slightly. Note that in shot E46363, injection of the tangential NBs stops briefly at $t = 7.3$, 9.5, 10.4, and 13.2 s, as seen in Fig. 3. At each interruption, the mode frequency is briefly reduced and soon recovers. The frequency change due to the interruptions is not clear in Fig. 5 (a), suggesting that the frequencies of the 2/1 and 3/2 modes change at a similar rate. This could be due to the fact that the profile of torque input by the tangential NBs is much broader than that of the EC-driven current.

3. Transition of Mode Frequency

As shown in the previous section, the mode frequency decreases with increasing mode amplitude; that is, the degree of the deceleration increases with the island width. To investigate the mode behavior at lower mode frequencies, EC waves were injected before the mode frequency saturated. Figure 6 (a) shows the temporal evolution of the normalized beta and the injection power of the NB and EC waves, and Fig. 6 (b) shows the frequency spectrum of magnetic perturbations. The discharge scenario is almost the same as that in Fig. 1. In the time window of Fig. 6 (a)–(c), the plasma is rotated in the counter-direction by tangential NBs of about 4 MW (the total NB power is 11.6 MW). The mode frequency gradually decreases with the misaligned ECCD from $t = 9.5$ s, and it suddenly decreases at $t \sim 10.4$ s, i.e., 0.9 s after the ECCD. Note that the mode frequency does not reach zero but remains low (~ 0.5 kHz). After the EC wave injection is turned off at $t = 11.5$ s, the mode frequency starts increasing at $t \sim 12.1$ s, i.e., 0.6 s after the turnoff, and saturates at a frequency similar to that before the ECCD. It can be speculated from the results in the previous section that the rotation velocity also changes during this phase. However, the toroidal rotation velocity is not available because an NB for CXRS measurement was not injected.

Figure 6 (d) shows the temporal evolution of the electron temperature at $t = 11$ s near and across the magnetic island measured with an electron cyclotron emission (ECE) diagnostic. The electron temperature oscillates regularly with a frequency of about 0.5 kHz, and the phase of the oscillations is inverted between 3.63 and 3.77 m. Furthermore, higher-harmonic oscillations, which are a characteristic waveform near the island center, are observed at 3.72 m. These facts show that rotating islands exist even in this phase.

The location and width of magnetic islands can be traced by the ECE diagnostic, and this method has been proven to be effective in tracing the island behavior [1, 10,

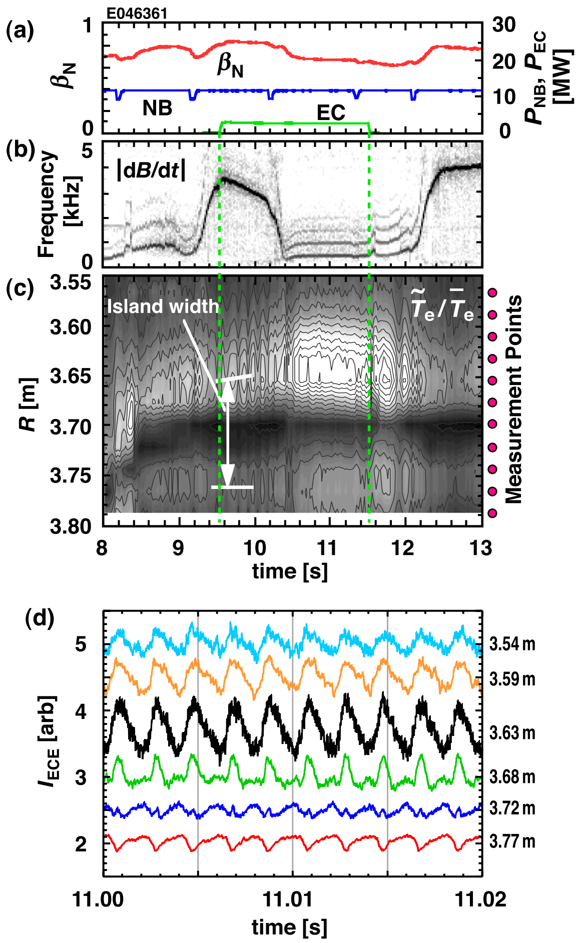

Fig. 6 Typical discharge of NTM destabilization by misaligned ECCD. (a) Normalized beta and injection power of the NB and EC waves, (b) frequency spectrum of magnetic perturbation, (c) contour plot of electron temperature perturbation and (d) temporal evolution of ECE intensity.

13, 14]. The temporal evolution of the island width in shot E46363 is shown in Fig. 6 (c), where the mode amplitude at each channel is plotted as a contour plot, and lighter regions correspond to larger mode amplitudes. In this contour plot, the distance between the two peaks corresponds to the full island width, and the local minimum point between the two peaks corresponds to the island center. During the ECCD, the island center is located at R = 3.69 m and is almost unchanged. The full island width before the ECCD is about 11 cm, and it slightly increases after the ECCD because of the destabilization effect. The width is almost unchanged during the ECCD. Just after the ECCD is turned off, the island width decreases, while the mode frequency stays at 0.5 kHz for about 0.6 s, as described above. From this observation, it can be concluded that the sudden decrease and increase in the mode frequency are not attributed to a sudden change in the island width.

Figure 7 shows the evolution of the mode frequency versus the island width. After a misaligned ECCD, the mode frequency gradually decreases with increasing island

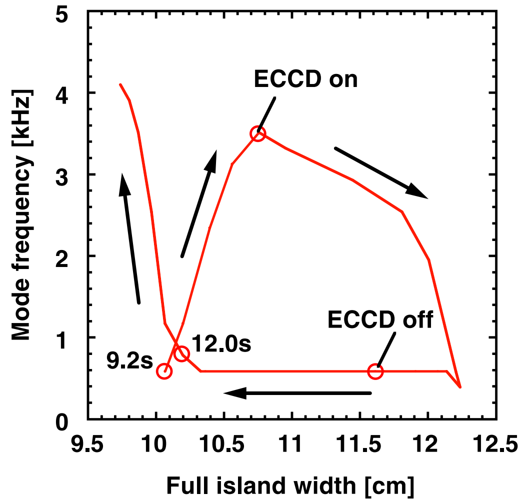

Fig. 7 Temporal evolution of the 2/1 mode frequency versus the full island width. NB power is fixed at 11.6 MW during the cycle.

width and then suddenly jumps to a low value. After the EC waves are turned off, the island width decreases while the mode frequency remains almost the same. The island widths at $t \sim 9.2$ s and ~ 12.0 s, at which the upward transition occurs, are similar. After the transition, the mode frequency increases to nearly the same value as that before the ECCD. The figure also shows that there is a hysteresis in the island width at which the downward and upward transitions occur. This suggests that once the transition occurs, the island width must be decreased further to rotate the mode again.

4. Summary and Discussion

The effect of magnetic islands associated with m/n = 2/1 NTMs on plasma rotation has been investigated. The magnetic island width was controlled by slightly changing the ECCD location to stabilize or destabilize the NTMs. Such a method has not been demonstrated before and is closer to the situation of growing or shrinking NTM islands than that of using external magnetic perturbation coils, in the sense that only the island at the mode rational surface is affected. In addition, although low-density locked modes in Ohmic discharges had been extensively investigated using external magnetic coils, the behavior of NTM islands at large magnetic islands was not investigated in detail. Furthermore, in the experiments described in this paper, the evolution of magnetic island structure has been measured using an ECE diagnostic in addition to magnetic perturbation measurement. The ECE diagnostic proves useful especially at low frequencies, where the signal-to-noise ratio of magnetic perturbation measurement generally becomes low.

This series of experiments showed that for the rotating NTM islands, the toroidal rotation velocity decreases slightly with increasing island width: 5.5 kHz for an island width of 0 cm (i.e., a completely stabilized island) and 3 kHz for a full island width of about 15 cm (~15% of the minor radius). A rapid decrease in the mode frequency, or an event like a transition, has been observed when the 2/1 NTM is destabilized for a mode frequency lower than that in the above experiments. Note that the torque input by NBs is the same as in the above cases. The ECE diagnostic showed that the island structure is sustained even in the low-frequency phase, and that the change in the full island width is about 0.5 cm. A rapid increase in the mode frequency about 0.5 s after the turnoff of the misaligned EC wave injection has also been observed. The upward transition occurs when the full island width became about 10 cm, which is about 20% smaller than the size at the downward transition. The result shows that there is a hysteresis in the downward and upward transitions.

Next, we consider the above two results simultaneously. With decreasing island width, the mode frequency reaches about 5.5 kHz, as shown in Fig. 4 (b). This frequency is considered to be the natural rotation frequency of the plasma. As shown in Fig. 7, the downward transition occurs at about 2.7 kHz. Thus, the transition occurs when the mode frequency decreases to about half the natural frequency. Note that the initial conditions of the two trajectories in Figs. 4 (b) and 7 are different, and that the trajectories cannot be connected. The interaction between magnetic islands and the external structure has been theoretically investigated [15], and the validity was confirmed for classical tearing mode islands in low-β discharges [16, 17]. According to the above model, the mode frequency, f, in the high-frequency state is described as $f/f_0 = 0.5\left(1 + \sqrt{1 - \tilde{B}^2/\tilde{B}_0^2}\right)$. Here, f_0 and $\tilde{B}_0$ are constants at fixed plasma parameters and correspond to the natural mode frequency and the mode amplitude at the transition, respectively. Least-square fitting shows that the values of f_0 and $\tilde{B}_0$ are 5.3 and 5.2, respectively, for the fitting of the experimental data shown in Fig. 4 (b), where the units of f and $\tilde{B}$ are kHz and an arbitrary unit, respectively. As this figure shows, the function fits the experimental island evolutions well, suggesting that the model can also be applied to NTM islands.

Acknowledgements

This study was partially supported by a Grant-in-Aid for Young Scientists (B) #22760662 from MEXT Japan.

[1] A. Isayama, Y. Kamada, N. Hayashi *et al.*, Nucl. Fusion **43**, 1272 (2003).
[2] K. Nagasaki, A. Isayama, S. Ide *et al.*, Nucl. Fusion **43**, L7 (2003).
[3] A. Isayama, G. Matsunaga, T. Kobayashi *et al.*, Nucl. Fusion **49**, 055006 (2009).
[4] M. Maraschek, G. Gantenbein, Q. Yu *et al.*, Phys. Rev. Lett. **98**, 025005 (2007).
[5] R. Prater, R.J. La Haye, T.C. Luce *et al.*, Nucl. Fusion **47**, 371 (2007).
[6] T.C. Hender, R. Fitzpatrick, A.W. Morris *et al.*, Nucl. Fusion **32**, 2091 (1992).
[7] R.J. La Haye, A.W. Hyatt and J.T. Scoville, Nucl. Fusion **32**, 2119 (1992).
[8] ITER Physics Basis Editors and ITER Physics Expert Group, Nucl. Fusion **39**, 2137 (1999).
[9] R.J. La Haye, A. Isayama and M. Maraschek, Nucl. Fusion **49**, 045005 (2009).
[10] A. Isayama, N. Oyama, H. Urano *et al.*, Nucl. Fusion **47**, 773 (2007).
[11] K. Hamamatsu and A. Fukuyama, Plasma Phys. Control. Fusion **42**, 1309 (2000).
[12] K. Tani, M. Azumi and R.S. Devoto, J. Comp. Phys **98**, 332 (1992).
[13] A. Isayama, Y. Kamada, T. Ozeki *et al.*, Plasma Phys. Control. Fusion **41**, 35 (1999).
[14] A. Isayama and the JT-60 Team, Phys. Plasmas **12**, 056117 (2005).
[15] R. Fitzpatrick, Nucl. Fusion **33**, 1049 (1993).
[16] D.A. Gates and T.C. Hender, Nucl. Fusion **36**, 273 (1996).
[17] P.C. de Vries, G. Waidmann, A.J. H Donné *et al.*, Plasma Phys. Control. Fusion **38**, 467 (1996).